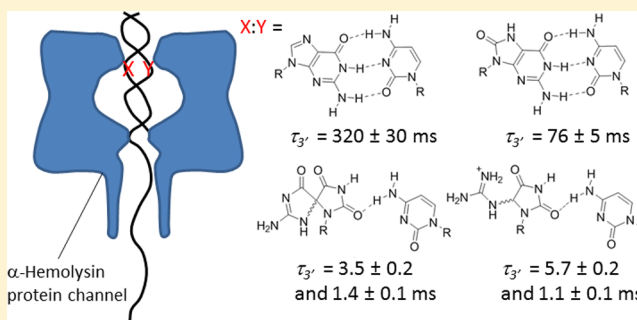# Structural Destabilization of DNA Duplexes Containing Single-Base Lesions Investigated by Nanopore Measurements

Qian Jin, Aaron M. Fleming, Yun Ding, Cynthia J. Burrows,* and Henry S. White*

Department of Chemistry, University of Utah, 315 South 1400 East, Salt Lake City, Utah 84112-0850, United States

S *Supporting Information*

ABSTRACT: The influence of DNA duplex structural destabilization introduced by a single base-pair modification was investigated by nanopore measurements. A series of 11 modified base pairs were introduced into the context of an otherwise complementary DNA duplex formed by a 17-mer and a 65-mer such that the overhanging ends comprised poly(dT)$_{23}$ tails, generating a representative set of duplexes that display a range of unzipping mechanistic behaviors and kinetic stabilities. The guanine oxidation products 8-oxo-7,8-dihydroguanine (OG), guanidinohydantoin (Gh), and spiroiminodihydantoin (Sp) were paired with either cytosine (C), adenine (A), or 2,6-diaminopurine (D) to form modified base pairs. The mechanism and kinetic rate constants of duplex dissociation were determined by threading either the 3′ or 5′ overhangs into an α-hemolysin (α-HL) channel under an electrical field and measuring the distributions of unzipping times at constant force. In order of decreasing thermodynamic stability (as measured by duplex melting points), the rate of duplex dissociation increases, and the mechanism evolves from a first-order reaction to two sequential first-order reactions. These measurements allow us to rank the kinetic stability of lesion-containing duplexes relative to the canonical G:C base pair in which the OG:C, Gh:C, and Sp:C base pairs are, respectively, 3−200 times less stable. The rate constants also depend on whether unzipping was initiated from the 3′ versus 5′ side of the duplex. The kinetic stability of these duplexes was interpreted in terms of the structural destabilization introduced by the single base-pair modification. Specifically, a large distortion of the duplex backbone introduced by the presence of the highly oxidized guanine products Sp and Gh leads to a rapid two-step unzipping. The number of hydrogen bonds in the modified base pair plays a lesser role in determining the kinetics of duplex dissociation.

X:Y =

$\tau_{3'} = 320 \pm 30$ ms

$\tau_{3'} = 76 \pm 5$ ms

$\tau_{3'} = 3.5 \pm 0.2$ and 1.4 ± 0.1 ms

$\tau_{3'} = 5.7 \pm 0.2$ and 1.1 ± 0.1 ms

α-Hemolysin protein channel

In biological cells, DNA nucleotides undergo continuous modification into lesions either spontaneously or by exposure to DNA damaging agents.[1] The damage occurs at a surprisingly high rate of tens of thousands of times per cell per day.[2] Although the majority of lesions are corrected by repair enzymes, damage beyond the cell's repair capability may lead to cell death or to cancer, cardiovascular, and age-related diseases.[3,4] One of the most common forms of DNA damage results from oxidizing free radicals that target the DNA base guanine (G) because it has the lowest redox potential.[5] Initial oxidation of G gives rise to 8-oxo-7,8-dihydroguanine (OG), a biomarker for monitoring oxidative stress in the cell. Moreover, OG is prone to further oxidation that yields either spiroiminodihydantoin (Sp) or guanidinohydantoin (Gh), depending on the reaction context.[6] The importance of these lesions on the thermodynamic stability of double-stranded DNA is fairly well established;[7−10] however, the influence of lesions on the kinetics of unraveling (i.e., unzipping) is less well studied.

The unzipping of duplex DNA has been investigated to gain insight into the process of strand separation during DNA replication and transcription.[11−13] Our groups have used the nanopore approach to induce the unzipping of lesion-containing dsDNA and to study the kinetic stability of damaged duplexes.[14] A preliminary report from our laboratories demonstrated that the force-induced strand dissociation of lesion-containing duplexes occurs by either a first-order reaction or two sequential first-order reactions, depending on the extent of the destabilizing effect imparted by the damage.[15] Here, the nanopore method is used to investigate the influence of a more extensive series of base modifications on duplex unzipping.

In single-molecule force experiments, the time-dependent trajectory describing the response of a biomolecule to an external force can be used to extract kinetic information concerning structures and interactions of individual molecules.[16,17] Kinetic studies using single-molecule force techniques have covered a variety of biological processes, including intramolecular and intermolecular interactions of DNA, RNA, and proteins.[18−21] Among them, the nanopore method provides a fast and linker-free approach for molecular manipulation that overcomes some of the drawbacks of optical tweezers and atomic force microscopy (AFM).[22−24] In a

65-mer: 5'-$(T)_{23}$-TTGGAGCTG**X**TGGCGTAGG-$(T)_{23}$
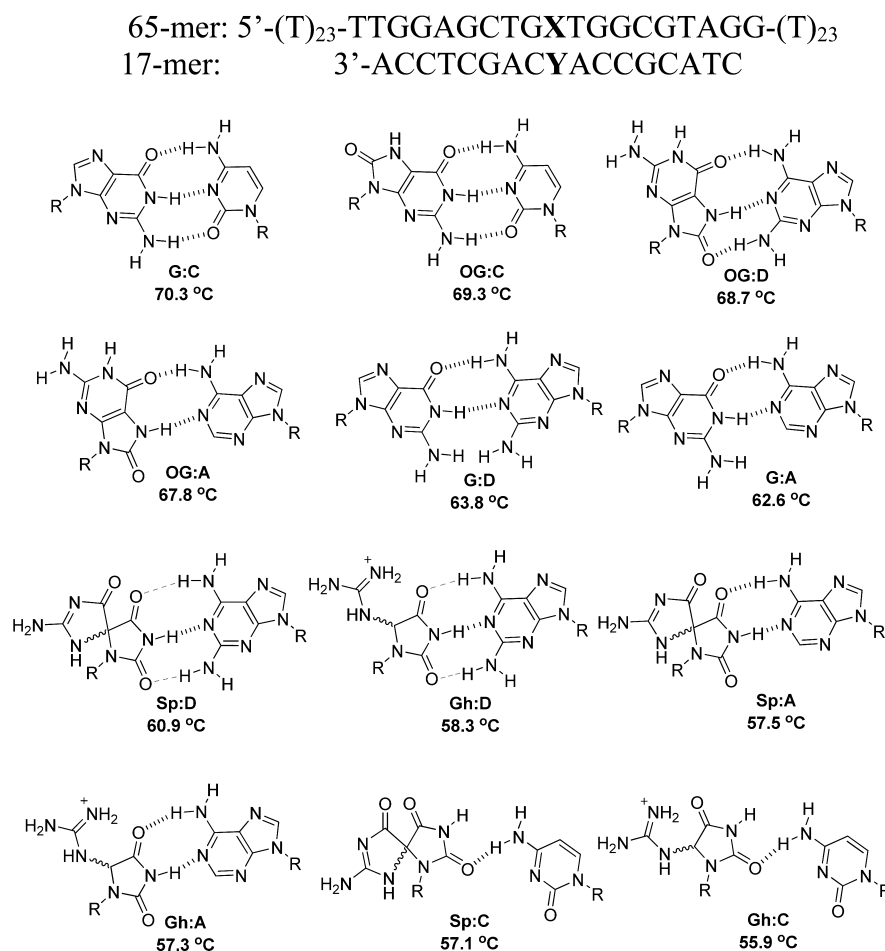17-mer: 3'-ACCTCGAC**Y**ACCGCATC

Figure 1. Base-pairing schemes for X:Y (X = G, OG, Sp, or Gh and Y = C, A, or D). The base pairs G:A, G:C, OG:A, and OG:C are drawn on the basis of reported structural data, whereas the hydantoin base pairs are drawn on the basis of predictions in refs 6 and 38. The duplexes are arranged in order of decreasing melting temperatures (from top down). The D-containing base pairs are predicted on the basis of their H-bonding capabilities as discussed in the text. The melting temperatures are listed under each X:Y-containing duplex and have an average standard deviation of 0.6 °C (see the Supporting Information for individual standard deviations in T_m).

nanopore experiment using the α-hemolysin (α-HL) nanopore, individual DNA duplexes are driven electrophoretically into the pore with only the overhang, if any, being able to fully thread past the constriction zone into the β-barrel.[25] In this experiment, the electrical field imposes a localized rupture force on the duplex, causing strand dissociation to occur.[26,27] From the moment of entry to that of rupture, the duplex generates a temporal blockade to the ionic current passing through the channel (carried by the electrolyte ions, K^{+} and Cl^{−}). The duration of this current blockage is used to extract kinetic information related to strand dissociation.[28−30] Typically, the unzipping duration of a double-stranded DNA within the α-HL channel is 2 to 3 orders of magnitude longer than the translocation time of single-stranded DNA (ssDNA) at the same applied voltage.[31,32]

Base pairs for G and its oxidation products OG, Sp, and Gh were inserted into a 17-mer duplex DNA (Figure 1). The base-pairing partner was systematically changed to probe the effect on the unzipping kinetics. This allowed us to interrogate the structural features that govern the kinetic stability of lesion-containing base pairs. Each of the base pairs was placed at a mutational hot spot in a portion of the K-ras gene sequence surrounding codon 12, a known location for oxidative damage to G nucleotides.[33,34] Eleven base-pair modifications (X:Y)

were chosen for study in this work, generating a broad range of variation concerning the extent of destabilizing effects: OG, or one of its second-stage oxidized products, Gh or Sp, was incorporated to introduce destabilization of different levels, whereas cytosine (C), adenine (A), or 2,6-diaminopurine (D) was paired with the lesion to adjust further the extent of destabilization.[35−37] The base D, an analog of A, can increase H bonding in X:Y compared with A pairing and can thus be used as a base-pair modulator.

■ **MATERIALS AND METHODS**

DNA Preparation and Purification Procedures. The oligodeoxynucleotides were synthesized from commercially available phosphoramidites (Glen Research, Sterling, VA) by the DNA-Peptide Core Facility at the University of Utah. Each oligodeoxynucleotide was cleaved from the synthetic column after synthesis and then deprotected according to the manufacturer's protocol. The oligonucleotides were purified using an ion-exchange HPLC column with a linear gradient of 25−100% B over 30 min while monitoring UV/vis absorbance at 260 nm (A = 10% CH_3CN/90% ddH_2O, B = 20 mM NaP_i, 1 M NaCl, pH 7, in 10% CH_3CN/90% ddH_2O, flow rate =1 mL/min). The Gh- and Sp-containing DNAs were synthesized following a previously established protocol from ref 10.

Thermal-Denaturation Experiments. Thermal-denaturation experiments to determine the T_m values were conducted with the truncated 23-mer strand 5′-TT TTG GAG CTG XTG GCG TAG GTT-3′ in which X = G, OG, Sp, or Gh. By removing the poly dT tails of the 65-mer stand, the hyperchromic shift for the transition from dsDNA to ssDNA was more clearly observed. The dsDNA samples were formed by mixing the 23-mer and 17-mer (3′-ACC TCG ACY ACC GCA TC-5′, Y = C, A, or D) in a 1:1 ratio in 1 M KCl, 10 mM PBS, and 1 mM EDTA (pH 7.4) at a concentration of 10 μM. The dsDNAs were annealed in a 90 °C water bath for 5 min and then slowly cooled to room temperature over 3 h. Thermal-denaturation experiments were then conducted on diluted dsDNA samples at 1 μM in the same solution. Samples were thermally equilibrated at 20 °C for 20 min followed by heating to 95 °C at a rate of 0.5 °C/min. As the samples were heated, UV/vis absorbance readings were recorded at 260 nm every 30 s. The T_m was determined using a two-point average analysis.

Chemicals and Materials for Nanopore Measurement. Monomer wild-type α-HL (List Biological Laboratories) was dissolved in water at 1 mg/mL and stored at −80 °C. The lipid, 1,2-diphytanoyl-*sn*-glycero-3-phosphocholine (Avanti Polar Lipids), was dissolved in decane at 10 mg/mL before use. Glass nanopore membranes (GNMs) were fabricated using a benchtop method as described in ref 39 and then chemically modified with 2% (v/v) (3-cyanopropyl) dimethylchlorosilane in acetonitrile to produce a hydrophobic surface as the support structure for the lipid bilayer.[40,41] The 65-mer strands (5′-T$_{23}$-TTG GAG CTG XTG GCG TAG G-T$_{23}$-3′, X = G, OG, Sp, or Gh) were mixed with the 17-mer strands (3′-ACC TCG ACY ACC GCA TC-5′, Y = C, A or D) at 1:5 mol ratio (65-mer vs 17-mer) to form duplexes in 1 M KCl, 10 mM PBS, and 1 mM EDTA (pH 7.4). The 65-mer and 17-mer mixture was heated in a 90 °C water bath for 5 min and then slowly cooled to room temperature over 3 h.

Duplex Unzipping Current–Time Recording. All current–time recordings were collected using a custom built amplifier and data acquisition system (Electronic BioSciences Inc., San Diego, CA). The same solution to dissolve the DNA (1 M KCl, 10 mM PBS, and 1 mM EDTA at pH 7.4) was used as the electrolyte for ion-channel recordings as well as to fill up the electrolyte reservoir and the GNM capillary (orifice radius ~500 nm). A voltage of −120 mV (*cis* vs *trans*) was applied across the GNM/bilayer using Ag/AgCl electrodes placed inside and outside of the GNM capillary. A lipid bilayer was formed by painting the lipid/decane solution across the GNM orifice. A positive pressure was applied to the inside of the GNM capillary, allowing the lipid bilayer to be functional for protein channel reconstitution.[42] Protein monomers were added to the *cis* side of the nanopore and self-assembled into the lipid bilayer as the heptamer ion channel. After protein insertion, the duplex DNA sample was added to the electrolyte reservoir at a final concentration of 5 μM. A minimum of 300 unzipping events were collected for each DNA sample. The i−t recordings were filtered at 10 kHz and sampled at 50 kHz.

Data Analysis. Unzipping events were extracted using QuB (version 1.5.0.31). According to previously reported duplex unzipping experiments in ref 15, the blockades in the i−t traces that lasted longer than 0.5 ms were analyzed as duplex-unzipping events. Event durations shorter than 0.5 ms represent the translocation of the excess 17-mer strands (because of the 1:5 mixing ratio of 65-mer/17-mer) and are

not discussed in this work. The duplex-unzipping process was described by either a first-order reaction or two sequential first-order reactions, depending on the specific duplex sequence. The shape of the unzipping-duration (t) histogram was used to determine which kinetic model best describes the duplex unzipping. The unzipping rate constants (k for Type I or k_1 and k_2 for Type II) were obtained on the basis of a fit of the t histogram using the corresponding kinetic equations.

The kinetic equation for Type I histograms is (equation derivation in ref 15)

$$C/T = ke^{-kt}\Delta t \tag{1}$$

where C/T is event counts in a time increment Δt centered at time t divided by the total counts. In Type I, the unzipping time constant $\tau = k^{-1}$.

The kinetic equation for Type II histograms is (equation derivation in ref 15)

$$C/T = \frac{k_1 k_2}{k_2 - k_1}(e^{-k_1 t} - e^{-k_2 t})\,\Delta t \tag{2}$$

where k_1 and k_2 correspond to the rate constants for the first and second unzipping steps. For Type II, the time constants for the first and second steps, τ_1 and τ_2, can be calculated from $\tau_1 = k_1^{-1}$ and $\tau_2 = k_2^{-1}$. Because k_1 and k_2 are interchangeable in eq 2, the fit of this equation to the histograms does not allow assignment of the extracted rate constant values to step 1 or 2. Unzipping experiments using duplexes in which either the 5′ or 3′ poly(dT)$_{23}$ tail of the 65-mer oligomer is removed are necessary to identify k_1 and k_2 with the individual steps (the details of this analysis are presented in ref 15).

Histograms were plotted and fit using OriginPro (version 8.5.1). Density plots were generated using the data analysis program provided by Electronic Biosciences.

■ RESULTS AND DISCUSSION

In this study, the 65-mer target strand containing a guanine derivative of interest X (X = G, OG, Sp, or Gh) was hybridized with a 17-mer Y-containing (Y = C, A, or D) strand, forming a duplex with the base pair X opposite to Y (Figure 1). The resultant duplex is fully complementary except for the modified base pair X:Y. For the sake of brevity, the duplex is hereafter denoted simply as X:Y.

Ion-channel measurements were performed to record the unzipping of single molecules of the X:Y duplexes within the α-HL channel under the influence of an electrical field (Figure 2). The blockage events resulting from the occupation of the channel by the duplex yielded two distinct current levels, depending on whether the 3′- or 5′-poly(dT)$_{23}$ overhang initiated threading into the channel; we have previously determined that the more blocking current level is associated with 3′ entry of the duplex and the less blocking level with 5′ entry (the 3′ and 5′ directions refer to the ends of the 65-mer target strand).[15] As shown in Figure 3, histograms of the blockage current extracted from unzipping events for each double-overhang duplex do not display a general preference of entry direction; between ~40 and 60% of events correspond to 3′ entry. This result is in contrast to the reported biased entry preferred at the 3′ end for ssDNA and hairpins.[43,44] The histograms shown in Figure 3 also indicate that the current blockage levels are nearly independent of the identity of X:Y for G-, OG-, and Gh-containing duplexes. The Sp-containing duplexes, however, always generated shallower current block-
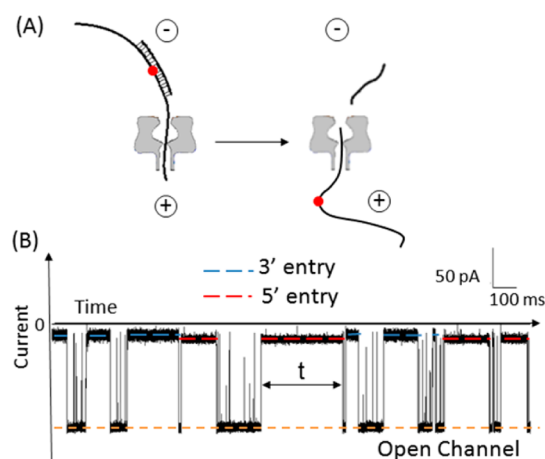
Figure 2. Unzipping of a DNA duplex using an α-HL nanopore under an electrical field. (A) dsDNA strand dissociation within an α-HL channel. The red dot in the target strand defines the relative position of X (X = G, OG, Sp, or Gh) opposite to Y (Y = C, A, or D) in the duplex. The + and − signs show the polarity of the electrodes. (B) Example of a current−time trace (X:Y = OG:C) at an applied voltage of −120 mV (cis versus trans). The blockades that last up to hundreds of milliseconds correspond to unzipping events of duplexes (unzipping duration shown as t). Events with duration shorter than 0.5 ms correspond to translocation of excess 17-mer ssDNA (the 65-mer and 17-mer strands are present in a 1:5 mol ratio). The red and blue dashed lines show the current blockage levels associated with 5′ and 3′ entry, respectively.
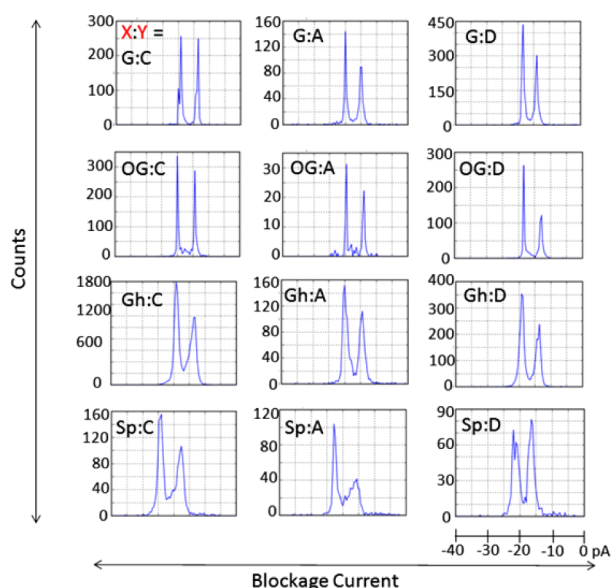

Figure 3. Histograms of the blockage current for the duplex formed by hybridizing the X-containing 65-mer with the Y-containing 17-mer at −120 mV. X:Y represents the modified base pair.

ages than the other duplexes by 3 to 5 pA, regardless of the pairing base or the entry direction. Broader current distributions were observed for all Gh- and Sp-containing duplexes, as expected on the basis of the conformational variations that originate from the coexistence of diastereomers for both Gh and Sp.[36,45]

Unzipping durations (t) sorted by entry direction (3′ vs 5′) were used to investigate the mechanism and kinetics of strand separation for each X:Y duplex. The histograms are consistent

with either a first-order reaction path (Type I) or a path comprising two sequential first-order reactions (Type II). In Figure 4, histograms of unzipping durations for the X:Y duplexes (X = G, OG, Sp, or Gh and Y = C or A) show a transition from the Type I exponential shape to the Type II peak shape as the T_m decreases, with the less stable duplexes tending to unzip more rapidly and in two steps. In cases where the strand dissociation follows a two-step model, the unzipping time constants are presented in Figure 4 without assignment of the first and second steps. Additional experiments using truncated duplexes that place X:Y asymmetrically in the sequence as demonstrated in ref 15 are necessary to determine the unzipping time constants for each step.

Well-defined Type II shapes of duration histograms were observed for Gh:C and Sp:C. Among the 12 base pair duplexes investigated here, Gh:C and Sp:C have the lowest T_m, suggesting that these duplexes are most capable of generating a pronounced energy well for the existence of an intermediate state.[23] In contrast, unzipping of the OG-containing duplex follows the Type I model, indicating that it is relatively stable despite the presence of the slightly destabilizing base pair. The histograms for Sp:A/D and Gh:A/D, whose stability is intermediate between the above cases, display shapes of either the Type I or the Type II model, consistent with the tendency of model evolution in terms of stability.

T_m values of the duplexes were used to order the histograms in Figure 4 to indicate the general correlation of thermodynamic and kinetic stabilities (decreasing from top to bottom). However, we cannot precisely predict the unzipping model or kinetic rates based merely on T_m, especially for duplexes of moderate stability.[46−49] Thus, instead of explaining the unzipping results using T_m values, we attempt to compare the kinetic data in terms of two features of local duplex structures: (1) known duplex distortion induced by the X:Y base pair and (2) the number of hydrogen bonds between the modified base pair.

In considering the influence of duplex distortion on stability, we find that the unzipping duration is very sensitive to even a slight displacement of the backbone relative to the perfectly matched G:C duplex. The unzipping duration decreased by a factor of 3 to 4 as a result of substituting G:C with OG:C. (For G:C, $\tau_{3'} = 320 \pm 30$ ms and $\tau_{5'} = 290 \pm 20$ ms. For OG:C, $\tau_{3'} = 76 \pm 5$ ms and $\tau_{5'} = 110 \pm 10$ ms.) In the oxidized structure, the T_m decreased by 1 °C because of a subtle distortion in the sugar−phosphate backbone originating from the repulsion between the C8 oxo group of the base and the C4′ oxygen of the ribose.[50] In terms of discriminating G:C and OG:C, the nanopore method outrivals thermal-denaturation methods in which a modest 1 °C T_m (Figure 1) difference that exists between these two base pairs translates to a 3- to 4-fold increase in the rate of unzipping (Figure 4). In the OG:A base pair, the T_m decreased by 2.5 °C (Figure 1) relative to the G:C base pair, whereas the unzipping rate was highly directionally dependent and increased by 2−12-fold (Figure 4). From OG:C to OG:D, the kinetic stability did not change unambiguously on the basis of either 3′ and 5′ entry. Although no structural details are available, we propose that OG adopts the syn conformation when paired with D, forming three H bonds (Figure 1).[51] Consequently, for OG:D, the tension between the C8 oxo group and the phosphate backbone is eased by rotating the C8 oxo group into the groove but not to the degree of a full recovery on the basis of the ~2 °C decrease in T_m observed for the OG:D base pair relative to the G:C base pair (Figure 1).
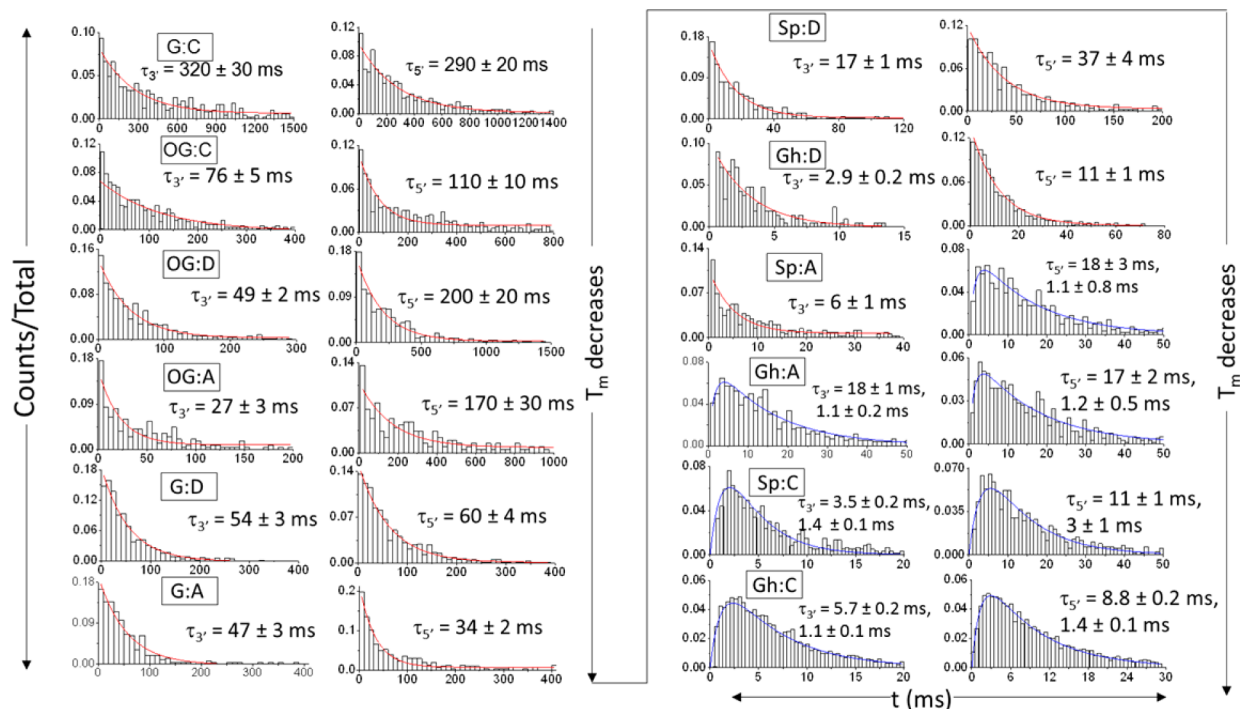
Figure 4. Histograms of unzipping time (t) via 3′ entry (left column) and 5′ entry (right column) at −120 mV for the duplex that contains X:Y (where X = G, OG, Gh or Sp and Y = C, A, D). The unzipping time constants (τ) were obtained on the basis of the fit (red or blue curves) of the t histograms using the corresponding kinetic model, either a first-order reaction (Type I, red) or two sequential first-order reactions (Type II, blue). If the strand dissociation follows the Type II model, then the unzipping time constants for each step are presented without assignment of the first and second steps. The histograms are plotted on different time scales to emphasize the shape as a determinant for the model type.

Further, by substituting OG:D/A with G:D/A, the decrease in durations were expected because of destabilization from widening of the phosphate backbone at the G:D/A mismatch site by ∼3 Å that is reflected in a ∼6 to 7 °C decrease in T_m relative to a G:C base pair (Figure 1).[52] For all Gh- and Sp-containing duplexes, experimental and theoretical studies have demonstrated that these nonplanar lesions cause serious distortions to the phosphate backbone as well as interruption of base stacking and hydrogen bonding, making them unzip much faster than G- and OG-containing duplexes.[38,53]

In cases where backbone distortion remains similar, the number of H bonds appears to determine the rate of duplex unzipping. The decrease in unzipping duration for OG:A versus OG:D, G:A versus G:D, and Sp:A versus Sp:D can be explained by reduction in the number of hydrogen bonds. Nevertheless, an exception occurs for Gh:A versus Gh:D (Figure 1). With fewer hydrogen bonds, Gh:A unzips slower than Gh:D, although the two-step model for Gh:A indicates that it is more destabilized than Gh:D. For Sp:C and Gh:C, in addition to forming poor H bonds between Gh/Sp and C, the incorporation of these two base pairs dramatically alters the duplex backbone, resulting in the most severe destabilizing effect observed. In view of the influence of backbone distortions and hydrogen bonding, backbone distortion that generates a large-scale structural perturbation (i.e., nonplanar lesions such as Sp and Gh) should facilitate unzipping more proficiently than removal of H-bonds whose effect is constrained mostly within the base pair. Thus, higher weight in determining the kinetic stability was assigned to the influence of distorting lesions over the number of hydrogen bonds in X:Y.

The results in Figure 4 confirmed that the sequence-dependent unzipping duration is also influenced by the unzipping direction. In Figure 4, for the duplexes in which the unzipping time constants for 3′ and 5′ entry are significantly different, unzipping from the 3′ end always proceeds faster than unzipping from the 5′ end. Furthermore, we found that the oxidized lesions destabilize the duplex in the 3′-orientation to a larger degree than the 5′-orientation, as evidenced by the more notable change of duration at 3′ entry for modified duplexes versus G:C. For example, by replacing G:C with the modified base pair OG:D, the unzipping duration decreased by a factor of 6.5 at 3′ entry and a factor of 1.5 at 5′ entry. (For G:C, $\tau_{3'}$ = 320 ± 30 ms and $\tau_{5'}$ = 290 ± 20 ms. For OG:D, $\tau_{3'}$ = 49 ± 2 ms and $\tau_{5'}$ = 200 ± 20 ms.)

In addition to studying the kinetics of strand separation in the nanopore, the results of unzipping duration also provide insight into the detection of damaged DNA products.[54−56] The mutagenic potentials of OG, Sp, and Gh make it important to detect them for the purpose of disease diagnosis and management.[57−61] We are able to differentiate target strands containing X = G, OG, Sp, or Gh using three different 17-mer probes, each containing Y = C, A, or D. The C probe destabilizes the target strand that contains oxidative lesions relative to the undamaged strand and causes the unzipping duration to decrease by 4 times for OG versus G and up to 60 times for Sp/Gh versus G. The stabilizing effect of D on OG relative to G enhances the detection selectivity toward OG and increases the unzipping duration for OG:D relative to G:D by a factor of 3 at 5′ entry. Specifically, Sp can be distinguished from G, OG, and Gh by inspecting the blockage current that results from its corresponding duplex.

CONCLUSIONS

The present nanopore-based experiments have demonstrated how the structural destabilization introduced by lesions influences the kinetic stability of dsDNA. A progression of the kinetic mechanism and rate has been observed from a single-step path of first-order kinetics to a path of two sequential first-order reactions, with the duplex containing the more destabilizing base pairs X:Y being prone to unravel in a two-step fashion. The kinetic properties of unzipping have been interpreted in terms of the degree of backbone distortion induced by the modified base pair, X:Y, as well as the number of hydrogen bonds within X:Y. Among the two factors mentioned here, the backbone distortion plays a major role in determining the stability of the duplex in α-HL. This study on duplexes with a broad range of structures leads us toward a better understanding of the physical models for the strand-separation process as well as provides new information about DNA local structures and interactions, which are often concealed in ensemble-averaged measurements. In addition, the wide selection of bases for pairing opposite a lesion, including synthetic heterocycles, allows us to have multiple options for tuning the properties of DNA and RNA assemblies in nucleic acids research. This work also sheds light on single-molecule damage detection by the ion-channel method using the unzipping concept in which one interrogates a specific sequence of a target strand with a customized probe.

ASSOCIATED CONTENT

Ⓢ Supporting Information

Melting temperatures for the duplexes, histogram of current blockage levels for a duplex containing both 3′- and 5′-overhangs, and unzipping time constants as a function of melting temperature. This material is available free of charge via the Internet at http://pubs.acs.org.

AUTHOR INFORMATION

Corresponding Authors
*E-mail: burrows@chem.utah.edu (C.J.B.).
*E-mail: white@chem.utah.edu (H.S.W.). Phone: 1-801-585-6256.

Notes
The authors declare no competing financial interest.

ACKNOWLEDGMENTS

REFERENCES

(1) Loeb, L. A., and Harris, C. C. (2008) Advances in chemical carcinogenesis: A historical review and prospective. *Cancer Res. 68*, 6863−6872.

(2) Mangal, D., Vudathala, D., Park, J. H., Lee, S. H., Penning, T. M., and Blair, I. A. (2009) Analysis of 7,8-dihydro-8-oxo-2′-deoxyguanosine in cellular DNA during oxidative stress. *Chem. Res. Toxicol. 22*, 788−797.

(3) Sohal, R. S., and Weindruch, R. (1996) Oxidative stress, caloric restriction, and aging. *Science 273*, 59−63.

(4) Zawia, N. H., Lahiri, D. K., and Cardozo-Pelaez, F. (2009) Epigenetics, oxidative stress, and Alzheimer disease. *Free Radicals Biol. Med. 46*, 1241−1249.

(5) Steenken, S., and Jovanovic, S. V. (1997) How easily oxidizable is DNA? One-electron reduction potentials of adenosine and guanosine radicals in aqueous solution. *J. Am. Chem. Soc. 119*, 617−618.

(6) Fleming, A. M., Muller, J. G., Dlouhy, A. C., and Burrows, C. J. (2012) Structural context effects in the oxidation of 8-oxo-7,8-dihydro-2′-deoxyguanosine to hydantoin products: Electrostatics, base stacking, and base pairing. *J. Am. Chem. Soc. 134*, 15091−15102.

(7) Plum, G. E., Grollman, A. P., Johnson, F., and Breslauer, K. J. (1995) Influence of the oxidatively damaged adduct 8-oxodeoxyguanosine on the conformation, energetics, and thermodynamic stability of a DNA duplex. *Biochemistry 34*, 16148−16160.

(8) Khutsishvili, I., Zhang, N., Marky, L. A., Crean, C., Patel, D. J., Geacintov, N. E., and Shafirovich, V. (2013) Thermodynamic profiles and nuclear magnetic resonance studies of oligonucleotide duplexes containing single diastereomeric spiroiminodihydantoin lesions. *Biochemistry 52*, 1354−1363.

(9) Yennie, C. J., and Delaney, S. (2012) Thermodynamic consequences of the hyperoxidized guanine lesion guanidinohydantoin in duplex DNA. *Chem. Res. Toxicol. 25*, 1732−1739.

(10) Kornyushyna, O., Berges, A. M., Muller, J. G., and Burrows, C. J. (2002) In vitro nucleotide misinsertion opposite the oxidized guanosine lesions spiroiminodihydantoin and guanidinohydantoin and DNA synthesis past the lesions using Escherichia coli DNA polymerase I (Klenow fragment). *Biochemistry 41*, 15304−16314.

(11) Bockelmann, U., Thomen, P., Essevaz-Roulet, B., Viasnoff, V., and Heslet, F. (2002) Unzipping DNA with optical tweezers: High sequence sensitivity and force flips. *Biophys. J. 82*, 1537−1553.

(12) Larson, M. H., Greenleaf, W. J., Landick, R., and Block, S. M. (2008) Applied force reveals mechanistic and energetic details of transcription termination. *Cell 132*, 971−982.

(13) Cocco, S., Monasson, R., and Marko, J. F. (2001) Force and kinetic barriers to unzipping of the DNA double helix. *Proc. Natl. Acad. Sci. U.S.A. 98*, 8608−8613.

(14) Schibel, A. E. P., Fleming, A. M., Jin, Q., An, N., Liu, J., Blakemore, C. P., White, H. S., and Burrows, C. J. (2011) Sequence-specific single-molecule analysis of 8-oxo-7,8-dihydroguanine lesions in DNA based on unzipping kinetics of complementary probes in ion channel recordings. *J. Am. Chem. Soc. 133*, 14778−14784.

(15) Jin, Q., Fleming, A. M., Burrows, C. J., and White, H. S. (2012) Unzipping kinetics of duplex DNA containing oxidized lesions in an α-hemolysin nanopore. *J. Am. Chem. Soc. 134*, 11006−11010.

(16) Rief, M., Gautel, M., Oesterhelt, F., Fernandez, J. M., and Gaub, H. E. (1997) Reversible unfolding of individual titin immunoglobulin domains by AFM. *Science 276*, 1109−1112.

(17) Bennink, M. L., Leuba, S. H., Leno, G. H., Zlatanova, J., de Grooth, B. G., and Greve, J. (2001) Unfolding individual nucleosomes by stretching single chromatin fibers with optical tweezers. *Nat. Struct. Mol. Biol. 8*, 606−610.

(18) Wang, M. D., Yin, H., Landick, R., Gelles, H., and Block, S. M. (1997) Stretching DNA with optical tweezers. *Biophys. J. 71*, 1335−1346.

(19) Li, P. T. X., Bustamante, C., and Tinoco, I. (2007) Real-time control of the energy landscape by force directs the folding of RNA molecules. *Proc. Natl. Acad. Sci. U.S.A. 104*, 7039−7044.

(20) Cecconi, C., Shank, E. A., Bustamante, C., and Marqusee, S. (2005) Direct observation of the three-state folding of a single protein molecule. *Science 309*, 2057−2060.

(21) Koch, S. J., Shundrovsky, A., Jantzen, B. C., and Wang, M. D. (2002) Probing protein-DNA interactions by unzipping a single DNA double helix. *Biophys. J. 83*, 1098−1105.

(22) Howorka, S., Movileanu, L., Braha, O., and Bayley, H. (2001) Kinetics of duplex formation for individual DNA strands within a single protein nanopore. *Proc. Natl. Acad. Sci. U.S.A. 98*, 12996−13001.

(23) Dudko, O. K., Mathé, J., Szabo, A., and Meller, A. (2010) Nanopore force spectroscopy tools for analyzing single biomolecular complexes. *Methods Enzymol. 475*, 565−589.

(24) Dudko, O. K., Mathé, J., Szabo, A., Meller, A., and Hummer, G. (2007) Extracting kinetics from single-molecule force spectroscopy: Nanopore unzipping of DNA hairpins. *Biophys. J. 92*, 4188−4195.

(25) Song, L., Hobaugh, M. R., Shustak, C., Cheley, S., Bayley, H., and Gouax, J. E. (1996) Structure of staphylococcal alpha-hemolysin, a heptameric transmembrane pore. *Science 274*, 1859−1865.

(26) Wanunu, M., Sutin, J., and Meller, A. (2009) DNA profiling using solid-state nanopores: Detection of DNA-binding molecules. *Nano Lett. 9*, 3498−3502.

(27) Howorka, S., Cheley, S., and Bayley, H. (2001) Sequence-specific detection of individual DNA strands using engineered nanopores. *Nat. Biotechnol. 19*, 636−639.

(28) Vercoutere, W., Winters-Hilt, S., Olsen, H., Deamer, D., Haussler, D., and Akeson, M. (2001) Rapid discrimination among individual DNA hairpin molecules at single-nucleotide resolution using an ion channel. *Nat. Biotechnol. 19*, 248−252.

(29) Vercoutere, W. A., Winters-Hilt, S., DeGuzman, V. S., Deamer, D., Ridino, S. E., Rodgers, J. T., Olsen, H. E., Marziali, A., and Akeson, M. (2003) Discrimination among individual Watson−Crick base pairs at the termini of single DNA hairpin molecules. *Nucleic Acids Res. 31*, 1311−1318.

(30) Mathè, J., Visram, H., Viasnoff, V., Rabin, Y., and Meller, A. (2004) Nanopore unzipping of individual DNA hairpin molecules. *Biophys. J. 87*, 3205−3212.

(31) Kasianowicz, J., Brandin, E., Branton, D., and Deamer, D. (1996) Characterization of individual polynucleotide molecules using a membrane channel. *Proc. Natl. Acad. Sci. U.S.A. 93*, 13770−13773.

(32) Akeson, M., Branton, D., Kasianowicz, J., Brandin, E., and Deamer, D. (1999) Microsecond timescale discrimination among polycytidylic acid, poly-adenylic acid, and polyuridylic acid as homopolymers or as segments within single RNA molecules. *Biophys. J. 77*, 3227−3233.

(33) Xie, Y., Yang, H., Cunanan, C., Okamoto, K., Shibata, D., Pan, J., Barnes, D. E., Lindahl, T., McIlhantton, M., Fishel, R., and Miller, J. H. (2004) Deficiencies in mouse Myh and Ogg1 result in tumor predisposition and G to T mutations in codon 12 of the K-ras oncogene in lung tumors. *Cancer Res. 64*, 3096−3102.

(34) Husgafvel-Pursiainen, K., Hackman, P., Ridanpaa, M., Anttila, S., Karjalainen, A., Partanen, T., Taikina-Aho, O., Heikkila, L., and Vainio, H. (1993) K-ras mutations in human adenocarcinoma of the lung: association with smoking and occupational exposure to asbestos. *Int. J. Cancer. 53*, 250−256.

(35) Luo, W., Muller, J. G., and Burrows, C. J. (2001) The pH-dependent role of superoxide in riboflavin-catalyzed photooxidation of 8-oxo-7,8-dihydroguanosine. *Org. Lett. 3*, 2801−2804.

(36) Luo, W., Muller, J. G., Rachlin, E. M., and Burrows, C. J. (2000) Characterization of spiroiminodihydantoin as a product of one-electron oxidation of 8-oxo-7,8-dihydroguanosine. *Org. Lett. 2*, 613−616.

(37) Luo, W., Muller, J. G., Rachlin, E. M., and Burrows, C. J. (2001) Characterization of hydantoin products from one-electron oxidation of 8-oxo-7,8-dihydroguanosine in a nucleoside model. *Chem. Res. Toxicol. 14*, 927−938.

(38) Jia, L., Shafirovich, V., Shapiro, R., Geacintov, N. E., and Broyde, S. (2005) Structural and thermodynamic features of spiroiminodihydantoin damaged DNA duplexes. *Biochemistry 44*, 13342−13353.

(39) Zhang, B., Galusha, J., Shiozawa, P. G., Wang, G., Bergren, A. J., Jones, R. M., White, R. J., Ervin, E. N., Cauley, C., and White, H. S. (2007) Bench-top method for fabricating glass-sealed nanodisk electrodes, glass nanopore electrodes, and glass nanopore membranes of controlled size. *Anal. Chem. 79*, 4778−4787.

(40) White, R. J., Ervin, E. N., Yang, T., Chem, X., Daniel, S., Cremer, P. S., and White, H. S. (2007) Single ion-channel recordings using glass nanopore membranes. *J. Am. Chem. Soc. 129*, 11766−11775.

(41) Lan, W.-J., and White, H. S. (2012) Diffusional motion of a particle translocating through a nanopore. *ACS Nano 6*, 1757−1765.

(42) Schibel, A. E. P., Heider, E. C., Harris, J. M., and White, H. S. (2011) Fluorescence microscopy of the pressure-dependent structure of lipid bilayers suspended across conical nanopores. *J. Am. Chem. Soc. 133*, 7810−7815.

(43) Mathé, J., Aksimentiev, A., Nelson, D. R., Schulten, K., and Meller, A. (2005) Orientation discrimination of single-stranded DNA inside the α-hemolysin membrane channel. *Proc. Natl. Acad. Sci. U.S.A. 102*, 12377−12382.

(44) Butler, T. Z., Gundlach, J. H., and Troll, M. (2007) Ionic current blockages from DNA and RNA molecules in the α-hemolysin nanopore. *Biophys. J. 93*, 3229−3240.

(45) Ye, Y., Muller, J. G., Luo, W., Mayne, C. L., Shallop, A. J., Jones, R. A., and Burrows, C. J. (2003) Formation of ^{13}C-, ^{15}N-, and ^{18}O-labeled guanidinohydantoin from guanosine oxidation with singlet oxygen. Implications for structure and mechanism. *J. Am. Chem. Soc. 125*, 13926−13927.

(46) McNally, B., Wanunu, M., and Meller, A. (2008) Electro-mechanical unzipping of individual DNA molecules using synthetic sub-2 nm pores. *Nano Lett. 8*, 3418−3422.

(47) Viasnoff, V., Chiaruttini, N., and Bockelmann, U. (2009) Probing DNA base pairing energy profiles using a nanopore. *Eur. Biophys. J. 38*, 263−269.

(48) Renner, S., Bessonov, A., Gerland, U., and Simmel, F. C. (2010) Sequence-dependent unfolding kinetics of DNA hairpins studied by nanopore force spectroscopy. *J. Phys.: Condens. Matter 22*, 454119.

(49) Viasnoff, V., Chiaruttini, N., Muzard, J., and Bockelmann, U. (2010) Force fluctuations assist nanopore unzipping of DNA. *J. Phys.: Condens. Matter 22*, 454122.

(50) Lipscomb, L. A., Peek, M. E., Morningstar, M. L., Verghis, S. M., Miller, E. M., Rich, A., Essigmann, J. M., and Williams, L. D. (1995) X-ray structure of a DNA decamer containing 7,8-dihydro-8-oxoguanine. *Proc. Natl. Acad. Sci. U.S.A. 92*, 719−723.

(51) Cheong, C., Tinoco, I., Jr., and Chollet, A. (1988) Thermodynamic studies of base pairing involving 2,6-diaminopurine. *Nucleic Acids Res. 16*, 5115−5122.

(52) Berashevich, J., and Chakraborty, T. (2009) Thermodynamics of G·A mispairs in DNA: Continuum electrostatic model. *J. Chem. Phys. 130*, 015101-1−015101-8.

(53) Aller, P., Ye, Y., Wallace, S. S., Burrows, C. J., and Doublié, S. (2010) Crystal structure of a replicative DNA polymerase bound to the oxidized guanine lesion guanidinohydantoin. *Biochemistry 49*, 2502−2509.

(54) Howorka, S., and Siwy, Z. (2009) Nanopore analytics: Sensing of single molecules. *Chem. Soc. Rev. 38*, 2360−2384.

(55) Wanunu, M., Cohen-Karni, D., Johnson, R. R., Fields, L., Benner, J., Peterman, N., Zheng, Y., Klein, M. L., and Drndic, M. (2010) Discrimination of methylcytosine from hydroxymethylcytosine in DNA molecules. *J. Am. Chem. Soc. 133*, 486−492.

(56) Schibel, A. E. P., An, N., Jin, Q., Fleming, A. M., Burrows, C. J., and White, H. S. (2010) Nanopore detection of 8-oxo-7,8-dihydro-2′-deoxyguanosine in immobilized single-stranded DNA via adduct formation to the DNA damage site. *J. Am. Chem. Soc. 132*, 17992−17995.

(57) Duarte, V., Muller, J. G., and Burrows, C. J. (1999) Insertion of dGMP and dAMP during in vitro DNA synthesis opposite an oxidized form of 7,8-dihydro-8-oxoguanine. *Nucleic. Acids. Res. 27*, 496−502.

(58) Hailer, M. K., Slade, P. G., Martin, B. D., and Sugden, K. D. (2005) Nei deficient Escherichia coli are sensitive to chromate and accumulate the oxidized guanine lesion spiroiminodihydantoin. *Chem. Res. Toxicol. 18*, 1378−1383.

(59) Delaney, S., Neeley, W. L., Delaney, J. C., and Essigmann, J. M. (2007) The substrate specificity of MutY for hyperoxidized guanine lesions in vivo. *Biochemistry 46*, 1448−1455.

(60) Henderson, P. T., Delaney, J. C., Muller, J. G., Neeley, W. L., Tannenbaum, S. R., Burrows, C. J., and Essigmann, J. M. (2003) The hydantoin lesions formed from oxidation of 7,8-dihydro-8-oxoguanine are potent sources of replication errors in vivo. *Biochemistry 42*, 9257−9262.

(61) Mangerich, A., Knutson, C. G., Parry, N. M., Muthupalani, S., Ye, W., Prestwich, E., Gui, L., McFaline, J. L., Mobley, M., Ge, Z., Taghizadeh, K., Wishnok, J, S., Wogan, G. N., Fox, J. G., Tannenbaum,

S. R., and Dedon, P. C. (2012) Infection-induced colitis in mice causes dynamic and tissue-specific changed in stress response and DNA damage leading to colon cancer. *Proc. Natl. Acad. Sci. U.S.A. 109*, 1820−1829.